




Düzce University Journal of Science & Technology

Research Article

Design and Control of Single-Phase Double-Stage PV-MPPT System

 Emre AVCI *

Department of Electrical-Electronics Engineering, Faculty of Engineering, Düzce University, Düzce, TURKEY

* Corresponding author's e-mail address: emreavci@duzce.edu.tr

DOI: 10.29130/dubited.1484226

ABSTRACT

In the double-stage Photovoltaic-Maximum Power Point Tracking (PV-MPPT) systems, the performance of each stage and the MPPT algorithm may affect the system performance. This study gives the design and control of a single-phase double-stage PV-MPPT system with a cascade controller. For the DC-link voltage control, a classical PI controller is employed. However, double-line frequency harmonic emerges inherently in the DC-link voltage. This voltage harmonic causes a third harmonic in the injected grid current. Therefore, a proportional multi-resonant controller is used in the inner current loop controller to control the grid current and suppress the third harmonic. The designed system's steady-state and dynamic performance are tested under different PV power and sudden power changes. The simulation results show that the injected grid current is in phase with the grid voltage and has a low THD value. Also, the DC-link voltage is stable under even sudden power changes. The results prove the effectiveness of the designed system.

Keywords: PV, Photovoltaic, Double-stage, MPPT, Grid

Tek-Fazlı Çift-Aşamalı FV-MGNT Sisteminin Tasarımı ve Kontrolü

ÖZET

Çift aşamalı Fotovoltaik-Maksimum Güç Noktası Takip (FV-MGNT) sistemlerinde her aşamanın ve MGNT algoritmasının performansı sistem performansını etkileyebilmektedir. Bu çalışma kaskat kontrolcülü tek-fazlı çift-aşamalı FV-MGNT sisteminin tasarım ve kontrolünü sunmaktadır. Dc bara gerilimi için klasik bir PI kontrolcüsüne yer verilmiş. Fakat DC bara geriliminde şebeke frekansının iki katı büyüklüğünde bir gerilim harmoniği doğal olarak ortaya çıkar. Bu nedenle, şebeke akımını kontrol etmek ve üçüncü harmoniği bastırmak için iç akım döngüsünde oransal çoklu rezonans kontrolörü kullanılmıştır. Tasarlanan sistemin kararlı durum ve dinamik performansı, farklı FV gücü ve ani güç değişimleri altında test edilmiştir. Simülasyon sonuçları, şebeke basılan akımının şebeke gerilimi ile aynı fazda olduğunu ve düşük bir THD değerine sahip olduğunu göstermektedir. Ayrıca DC bara gerilimi ani güç değişimlerinde kararlı kalmıştır. Sonuçlar tasarlanan sistemin etkinliğini kanıtlamaktadır.

Anahtar Kelimeler: FV, Fotovoltaik, Çift-Aşamalı, MGNT, Şebeke

I. INTRODUCTION

The global adoption of photovoltaic (PV) systems has witnessed remarkable growth over the past decade, spurred by increasing environmental concerns and the pursuit of sustainable energy solutions [1,2]. According to the International Energy Agency (IEA), the cumulative installed solar power capacity reached 1185 gigawatts (GW) in 2019. [3]. Government agencies frequently release forecasts for solar expansion, typically underestimating its growth. According to projections from the IEA, by 2050, solar PV capacity is expected to soar to 4.7 terawatts (4,674 GW) in its high-renewable scenario. With more than half of this capacity expected to be installed in China and India, solar power is anticipated to become the primary source of electricity worldwide [4]. This exponential expansion underscores the pivotal role of PV technology in the global energy landscape, with projections indicating a continued upward trajectory in installations in the foreseeable future[5].

As PV systems become increasingly prevalent in residential applications, the interest in single-phase grid-tied PV-MPPT systems is increasing [6]. Due to the low voltage output of the PV cells, double-stage current source grid-connected type topology is frequently utilized for a low-power output PV grid-connected inverter [7]. This topology consists of a PV array, a DC-DC boost converter, an inverter, and a filter between the grid and inverter. A Maximum Power Point Tracking (MPPT) algorithm extracts maximum power from the PV array. However, in the literature, the function of this algorithm in double-stage systems is achieved in two different methods, as shown in Fig.1 (a) and Fig.1 (b). In the former method, the boost converter controls DC-link voltage and the MPPT algorithm generates reference grid current amplitude (I^*). On the other hand, in the latter method, the output of the MPPT algorithm is duty cycle (d), which manipulates the boost converter to achieve the MPPT function. In both methods, it is expected from the inverter control stage that the injected grid current has a low Total Harmonic Distortion (THD) at unity power factor with high dynamic performance [8]. In [9], these two methods are compared, and it is clearly shown that although the DC-link voltage (v_{dc}) stability performance of the method in Fig. 1 (a) is higher, the MPPT performance is lower than the other method in Fig. 1 (b).

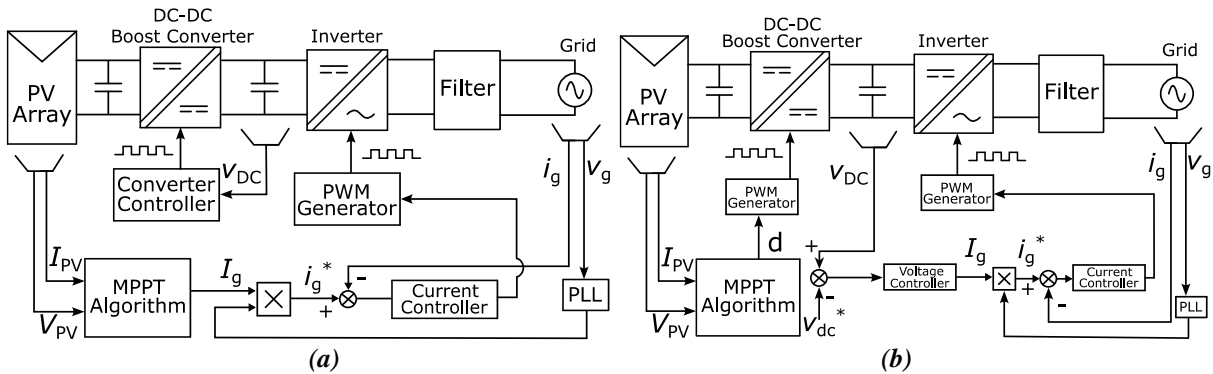


Figure 1. Different control techniques of the two-stage single-phase PV-MPPT system.

The energy-storage capacitor, known as the DC-link capacitor, is placed between these two stages, as depicted in Fig. 1. This capacitor is employed to support a stable DC-link voltage to the inverter filtering out the high-frequency harmonics from the DC-link. When the controller design for the voltage across this capacitor is done, two main problems should be considered for high-performance grid-tied single-phase PV-MPPT systems. The first is the inherent double grid frequency harmonic ($2\omega_1$) in the DC-link voltage, which causes the third harmonic content in the injected grid current. The second issue involves fluctuations in the DC-link voltage, mainly when there's a sudden change in PV power. This fluctuation should not exceed the rating of the system components. As a primitive solution, passive filtering can be applied using a large capacitance in the DC-link or between the PV array and the DC-DC converter. However, the larger capacitance causes an increasing size and cost of the system and reduces the dynamic and steady-state performance of the MPPT. Instead, more complicated passive filters can be employed, including more than one circuit element. Indeed, this also increases the size and cost of the system and makes it more complicated [10].

Typically, a cascaded controller technique controls both DC-link voltage and injected grid current. A Proportional-Integral (PI) controller is frequently used in the outer voltage loop control because the controlled variable is a DC signal. A PI controller with Clark/Park transformation can be implemented for the inner loop with zero steady-state error. Apart from these techniques, many different controller techniques for double-stage PV-MPPT systems can be found in the literature. In [11], adaptive, and in [12], an adjustable DC-link voltage controller is presented. In [13], a robust linear active disturbance rejection control technique is adopted for DC-link voltage control. In [14], the second harmonic in the bus voltage is eliminated by using cascade H-bridge multilevel converter topology with instantaneous power control technique. Another work in [15] proposes a flying capacitor average voltage control for handling with the second harmonics. In [16], a high-frequency four-winding transformer is employed for a modular three-phase PV system to hold power balance and voltage oscillation. Against this backdrop, this paper investigates the design and control aspects of single-phase double-stage PV-MPPT systems, focusing on addressing the evolving challenges posed by grid integration and power quality requirements. Leveraging insights from existing literature and empirical observations, the study aims to elucidate critical control methodologies, evaluate their efficacy in mitigating current distortion and harmonics, and propose novel strategies to enhance the performance and reliability of grid-connected PV systems.

By delving into the intricacies of system design and control, in this work, a single-phase double-stage grid-tied PV-MPPT system is designed with a double-loop cascade controller. A PI controller is employed to handle the second-order harmonics and voltage control of the DC link. For the inner current loop, a Proportional Multi Resonant (PMR) controller is selected for the pre-determined odd harmonics (e.g., 3rd and 5th) compensation to succeed in a high-performance MPPT system. The rest of the paper is organized as follows: in the next section, the modelling of each system stage is given. Section 3 provides the controller with the principle and design of the system. Section 4 shows detailed simulation results, and the work results are presented in the final section.

II. MODELLING OF THE SYSTEM

The system in this study is composed of the PV array, a boost-type DC-DC converter, an MPPT algorithm, an H-bridge 2-level single-phase inverter, and an LCL-type filter, as seen in Fig.2. In this section, the modelling of these parts of the system is detailed.

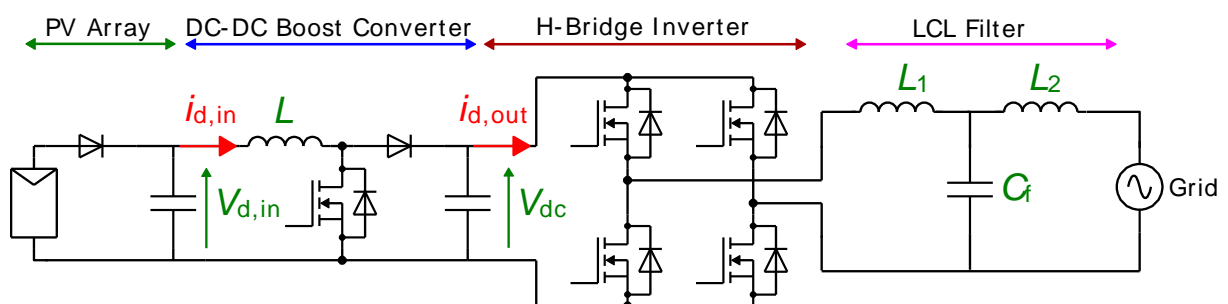


Figure 2. Different control techniques of the two-stage single-phase PV-MPPT system.

A. 1. PV Array Model

Photovoltaic (PV) systems, which convert sunlight into electrical power, play an essential role in sustainable energy solutions. The photovoltaic array is the heart of any PV system, comprised of linked solar panels such as Series-Parallel (SP). Each solar panel produces electrical energy reacting to incoming sunlight, resulting in a distinctive voltage-current (V-I) curve. The maximum power point on this curve represents the panel's peak efficiency. The Maximum Power Point Tracking (MPPT)

technique is critical for improving PV system efficiency. MPPT ensures that a solar panel runs at its maximum power point, optimizing energy gathering and improving overall system efficiency. This method continually analyses the PV array's electrical output and changes the operating point to guarantee that the system works at maximum power. The MPPT controller uses algorithms and control techniques to dynamically adjust to changing environmental factors, including sun irradiance and temperature.

To obtain appropriate voltage and power at the PV array output, the number of series (N_s) and the number of parallels (N_p) PV panels are configured. Within the single-diode model [17], the $N_s \times N_p$ configured PV array model is given in Fig.3. From the figure, the panel characteristic equation can be obtained as in Eq. 1, where I_{pv} and V_{pv} is the output current and voltage of the array, R_s and R_p is the equivalent series and shunt resistance, q is the electron charge, A is the diode quality factor and B is the Boltzmann constant.

$$I_{pv} = N_p I_{ph} - N_p I_D \left[\exp \left(q \frac{N_p V_{pv} + I_{pv} R_s N_s}{R_p B N_s A} \right) - 1 \right] - \frac{N_s I_{pv} R_s + N_p V_{pv}}{N_s R_p} \quad (1)$$

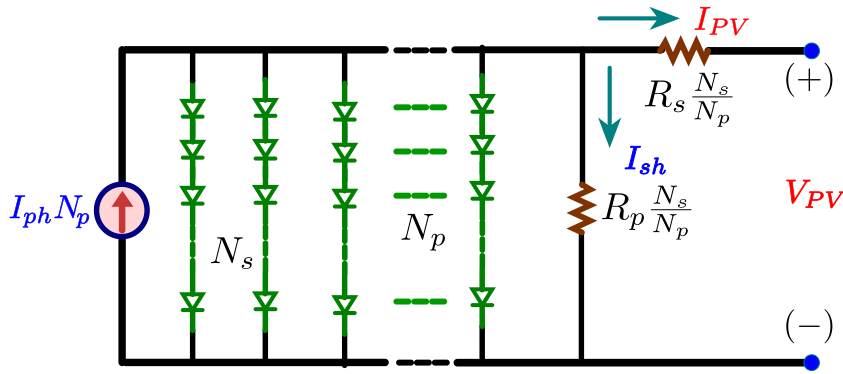


Figure 3. Single diode model of $N_s \times N_p$ configured PV array.

In this work, a 4×4 series-parallel configured array is created using a PV panel, whose parameters are listed in Table 1. The reference temperature of the panels is 25 C^0 , and the irradiation is 1000 W/m^2 .

Table 1. Parameters of the employed PV panel.

Parameter	Value
Maximum Power (P_{max})	215 W
Voltage at P_{max}	26.6 V
Current at P_{max}	8.09 A
Short-Circuit Current	8.78 A
Open Circuit Voltage	33.2 V

A. 2. DC-DC Converter Model

In the first stage of the system, a boost-type DC-DC converter is employed to arrange the PV array output voltage and power for the maximum power tracking and the second stage converter (inverter). As seen in Fig. 2, the output voltage of the PV array is filtered with C_{pv} capacitor. This voltage is the converter's input voltage, composed of a semiconductor switch, diode, and inductance. The relationship between the input and output of this converter in Continuous Conduction Mode (CCM) is given in Eq. 2, where $V_{d,in}$ and $I_{d,in}$ is the input voltage and current, $V_{d,out}$ and $I_{d,out}$ is the output voltage and current of the converter, d is the duty ratio of the PWM signal. The inductance value of the converter (L) can be

determined with Eq. (3), where ΔI_L is the current ripple of the inductance, f_{sw} is the switching frequency. To guarantee the CCM operation, Eq. 5, where I_{LB} the boundary current of the inductance, is also considered for the inductance value. When PV array power decreases with the changing environmental conditions, such as irradiation level, the boost converter can not guarantee the CCM operation. Therefore, this inductance value is critical for the system's performance. The converter parameters are designed with the given equations as in Table 2.

$$\frac{I_{d,in}}{I_{d,out}} = \frac{V_{d,out}}{V_{d,in}} = \frac{1}{1-d} \quad (2)$$

$$L = \frac{V_{d,in} \times (V_{d,out} - V_{d,in})}{\Delta I_L \times f_{sw} \times V_{d,out}} \quad (3)$$

$$\Delta I_L = \frac{d \times V_{d,in(min)}}{f_{sw} \times L} \quad (4)$$

$$I_{LB} = \frac{V_{d,out}}{2L \times f_{sw}} d(1-d) \quad (5)$$

A. 3. Grid-Tied Inverter Model with LCL Filter

At the output of the DC-DC converter, the DC-link power is transferred into the grid via an inverter meeting specific requirements and performances. Being an interface between the grid and inverter, the filter type is typically selected as a high-order LCL type because it provides sufficient performance, a simple design, and a smaller size. This study uses an H-bridge single-phase inverter with an LCL-type filter. Most conventional methods to design the filter parameters start with selecting the inverter side filter inductance (L_1). Therefore, Eq. (6) is employed for choosing the L_1 inductance, where V_g is the grid nominal voltage, P_r is the rated power of the converter, $I_{L1,ripple}$ is the current ripple of the L_1 . The sizing of the filter capacitor (C_f) is mainly determined according to the reactive power percentage ($\%Q_r$) supplied by the converter as in Eq. 7, where f_1 is the fundamental harmonic frequency of the grid. For a stable operation, the filter's resonance frequency (f_r), formulated in Eq.8, should be carefully designed. To provide this, the criteria $10f_1 < f_r < f_{sw}/2$ is adopted and used to size the grid side inductance (L_2) [18,19]. Designed with this information, the LCL filter parameters can be found in Table 2.

$$L_1 = \frac{V_{DC} \times V_g}{8 \times P_r \times f_{sw} \times \%I_{L1,ripple}} \quad (6)$$

$$C_f = \frac{\%Q_r}{2 \times \pi \times f_1 \times V_g^2} \quad (7)$$

$$f_r = \frac{1}{2\pi} \sqrt{\frac{L_1 + L_2}{L_1 L_2 C_f}} \quad (8)$$

Table 2. Parameters of the employed PV panel.

Parameter	Value
Inductance of the converter (L)	215 W
Capacitor of the converter (C)	26.6 V
Inverter-side inductance of the filter (L_1)	8.09 A
Grid-side inductance of the filter (L_2)	8.78 A
Capacitor of the converter (C_f)	33.2 V

III. CONTROLLER PRINCIPLE AND DESIGN

The proposed work achieves the MPPT strategy with the Perturb and Observer (P&O) algorithm with a fixed-step strategy and double-stage hardware configuration. The first stage of the system is a boost-type DC-DC converter controlled with the MPPT algorithm. The algorithm uses the measured array voltage (V_{pv}) and current (i_{pv}) to calculate the duty cycle (d) for the DC-DC converter by perturbing duty with a fixed step. With this, the MPPT function is achieved in the first stage. The second stage inverter achieves the DC link voltage control and grid synchronization with the double loop control strategy given in Fig. 4.

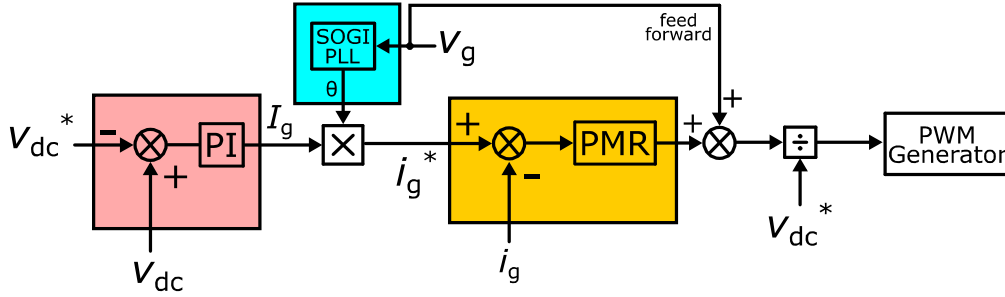


Figure 4. Double-loop proposed control strategy of the system.

It is aimed at the outer voltage loop that controls the DC-link voltage and stabilizes the vicinity of the reference DC voltage (v_{dc}^*). An increase in the DC link voltage is decreased by increasing the grid current reference amplitude (I_g) and vice versa. To do this, the measured DC bus voltage (v_{dc}) is subtracted from the reference voltage (v_{dc}^*). Then, the employed PI controller, whose transfer function ($G_{PI}(s)$) is given in Eq. 9, calculates the grid current reference amplitude (I_g). This process should balance power between the DC and AC sides of the system. However, because of the inherent characteristic of the single-phase system, a second harmonic ($2f_1$) appears on the DC bus voltage. This causes a third harmonic in the injected grid current [20]. This can be shown in Fig. 5, where Fast Fourier Transform (FFT) analysis of a double-stage single-phase PV-MPPT system's DC bus voltage and grid current is given. Therefore, this work uses the Proportional Resonant (PR) with the third and fifth harmonic compensators, called the Proportional Multi Resonant (PMR) controller. In Eq. 10 and 11, the PR and PMR controller transfer functions are given, respectively, where k_{pr} is the proportional part of the controller, w_c is the cut-off frequency, and h indicates harmonic order. As shown in Fig. 4, the grid voltage feed-forward term is also employed to increase system steady-state error.

$$G_{PI}(s) = k_p + \frac{k_i}{s} \quad (9)$$

$$G_{PR}(s) = k_{pr} + \frac{k_{i1}w_{c1}s}{s^2 + 2w_{c1}s + w_1^2} \quad (10)$$

$$G_{PMR}(s) = k_{pr} + \sum_{h=1}^{\infty} \left(\frac{k_{ih}w_{ch}s}{s^2 + 2w_{ch}s + w_h^2} \right) \quad (11)$$

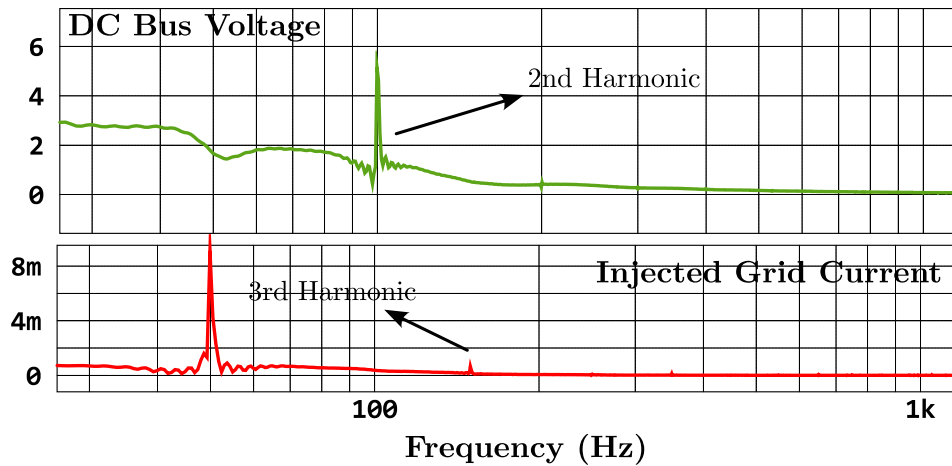


Figure 5. FFT analysis of the DC bus voltage and grid current.

The methods proposed in [21-23] are adopted to determine the parameters of the PMR-based inner loop current controller. For the design criteria of the controller, the phase and gain margins are selected as a minimum of 30 degrees and 2 dB, respectively. For the outer voltage loop controller design, the PSIM software-based trial-error method is used. The parameters of the designed controller are given in Table 3.

Table 3. Parameters of the designed controller.

Parameter	Value
Proportional part of the PI controller (k_p)	0.1
Integrator part of the PI controller (k_i)	10
Proportional part of the PMR controller (k_{pr})	10
Integrator part of the PMR controller ($k_{i1,3}$)	4000, 2000
Grid base frequency (w_1)	50 Hz
Natural Frequency of the PMR controller ($w_{c1,3}$)	2, 0.1

III. RESULTS

To demonstrate the effectiveness and performance of the designed 3.4 kW system, a double-stage single-phase PV-MPPT system has been built in PSIM simulation software as shown in Fig. 6. In the simulation step, the parameter settings of the program are as follows: Solver type is Fixed-step, the time step is 1e-6, and the sampling frequency is 20 kHz. The PV array and the hardware specifications are listed in Table 1 and Table 2, respectively.

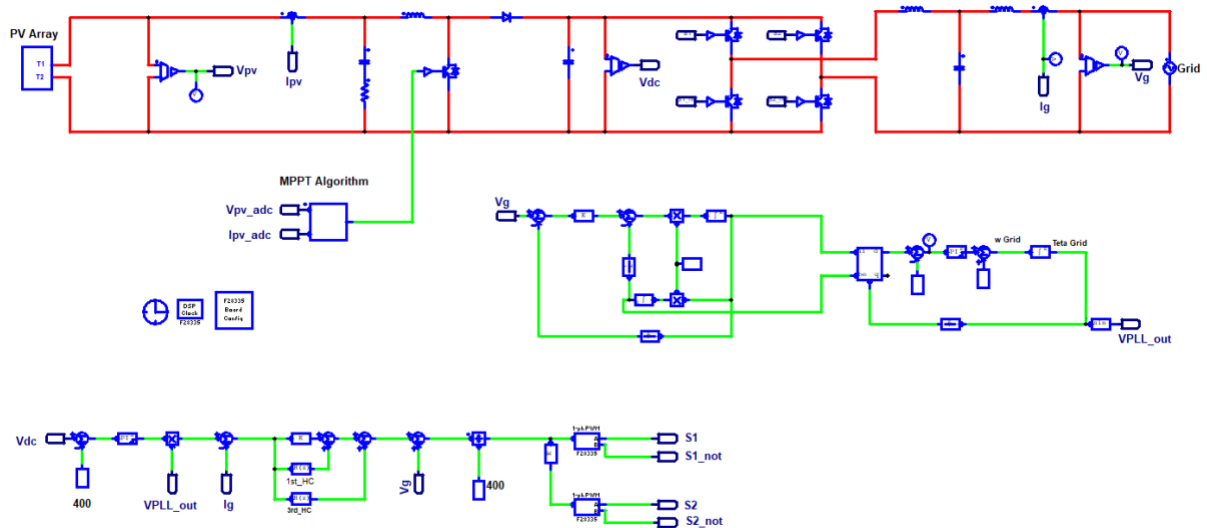


Figure 6. Simulated system model.

The first set of simulations is conducted under 1000 W/m^2 irradiation for the PV array, representing the rated power work. Fig. 7.a presents the grid voltage and scaled injected grid current (magnified 10 times) as the steady state. The figure shows that the injected grid current is in phase with grid voltage with almost unity power factor (0.9965). The Fast Fourier Transform analysis of the grid current can be seen in Fig.7.b with only the fundamental resonant (only PR) current controller. Fig. 7.b shows that the harmonic content of the grid current is composed of the third harmonic, which should be suppressed by the third harmonic resonant controller. The grid current has 5.71% Total Harmonic Distortion (THD) with this form.

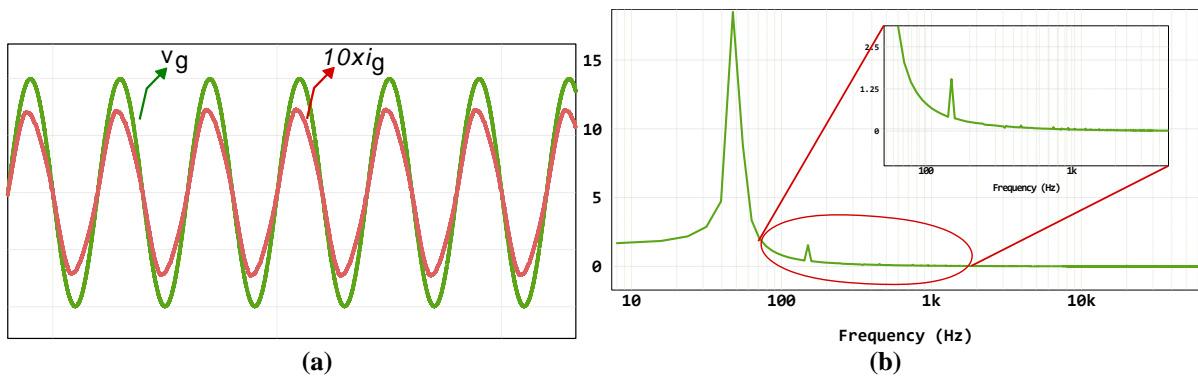


Figure 7. (a) grid voltage and current (volt/div: 311V, time/div:0.25sec) (b) FFT analysis of the grid current with only fundamental resonant controller.

With the third harmonic resonant, the grid current and DC-link voltage waveforms are given in Fig.8.a and Fig.8.b under the rated power (1000 W/m^2 irradiation), respectively. As can be seen there, the DC-link voltage has a 27V peak-to-peak fluctuation value because of the second harmonic in the voltage. The THD value of the grid current decreases to a 3.2% level, which exhibits the third harmonic resonant controller effect.

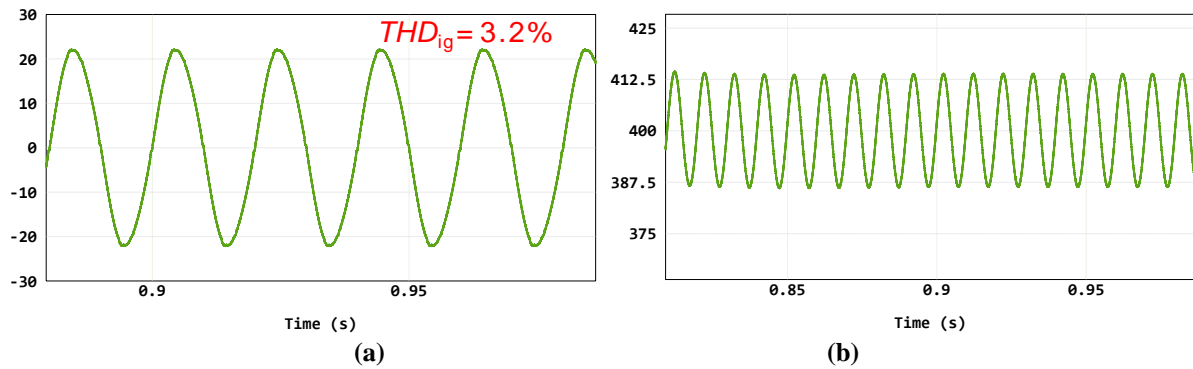


Figure 8. (a) grid current (current/div: 10A, time/div:0.05sec) and (b) DC-link voltage (volt/div=12.5V, time/div:0.05sec) with the first and third harmonic resonant controller under the rated power.

To test the dynamic performance of the system, the power of the system is decreased to half and then increased to the full rated power. For this reason, the PV array is first exposed to the 1000 W/m^2 irradiation, then changed to 500 W/m^2 and 1000 W/m^2 . In Fig.9.a and Fig.8.9, the DC-link voltage and grid current waveforms are given under changing power levels. As seen from Fig.9.a, the magnitude of the second harmonic in the DC-link voltage rises as the power increases. The DC-link voltage follows the reference 400 V. On the other hand, as seen in Fig.9.b, the power increase causes a decrease in the THD value of the grid current. Therefore, in Fig. 10.a and Fig. 10.b, the peak-to-peak voltage of the DC-link and the THD value of the grid current graphs are given, respectively, with respect to changing power levels.

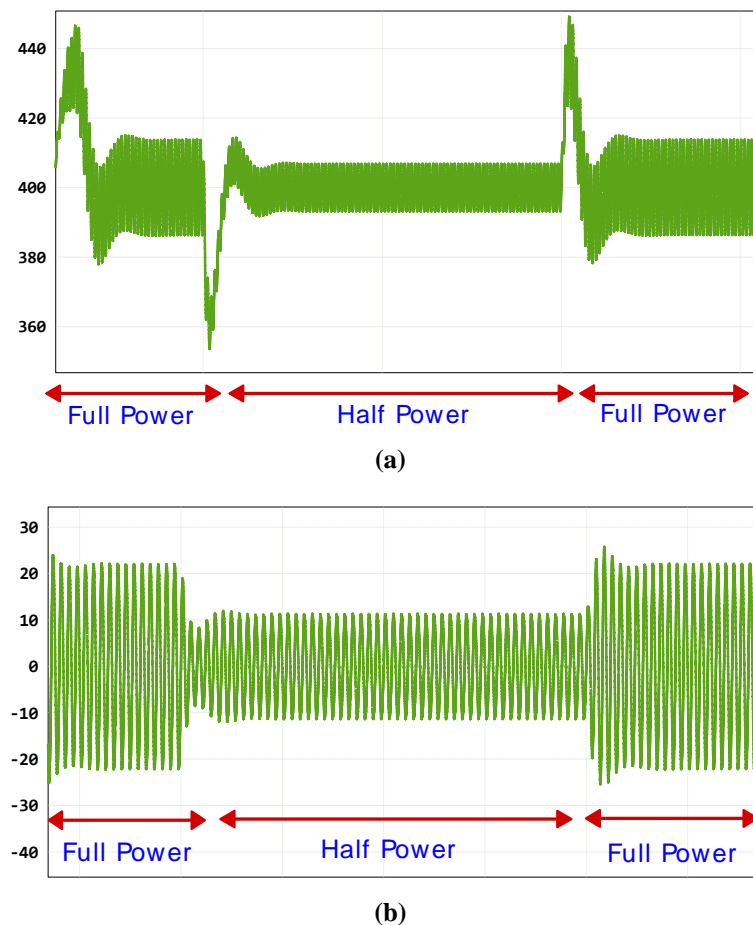


Figure 9. Dynamic system performance (a) DC-link voltage and (b) grid current with changing PV power level.

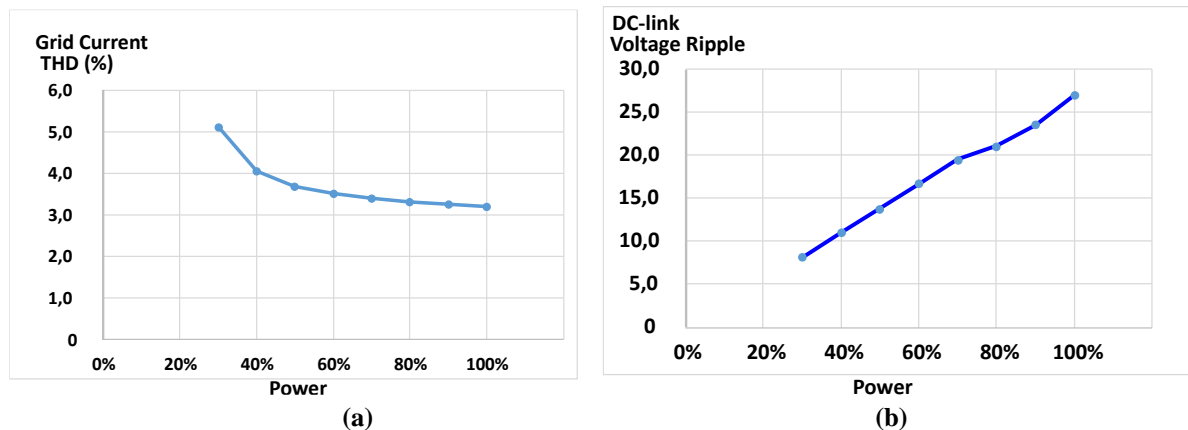


Figure 10. (a) grid current THD and (b) DC-link peak-to-peak voltage oscillation under different power levels.

IV. CONCLUSION

This article presents the controller design of the double-stage single-phase PV-MPPT system. The employed cascade (double-loop) control strategy includes DC-link voltage and grid current control. In the out loop, a simple PI controller is used. The third harmonic in the grid current caused by the double line frequency harmonics in the DC-link voltage is suppressed with the PMR controller. The simulation results confirm that the generated PV power is injected into the grid with a unity power factor and fulfills the high-performance criteria. In future work, it can be done that the DC-link voltage oscillations and grid current harmonics are reduced to a low level, even at low operating powers.

V. REFERENCES

- [1] Elibol, E., & Dikmen, O. (2024). Long-term performance investigation of different solar panels in the West Black Sea Region. *Clean Technologies and Environmental Policy*, 26(3), 875-899.
- [2] Oguz, C. B., Avci, E., & Ozturk, S. B. (2023). Analysis of PV power plant performance considering combination of different MPPT algorithms, shading patterns and connection types. *Engineering Science and Technology, an International Journal*, 48, 101559.
- [3] Jäger-Waldau, A. (2023). Snapshot of photovoltaics– May 2023. *EPJ Photovoltaics*, 14, 23.
- [4] Metayer, M., Breyer, C., & Fell, H. J. (2015, September). The projections for the future and quality in the past of the World Energy Outlook for solar PV and other renewable energy technologies. In *31st European Photovoltaic Solar Energy Conference and Exhibition (Vol. 5)*.
- [5] Wolniak, R., & Skotnicka-Zasadzień, B. (2022). Development of photovoltaic energy in EU countries as an alternative to fossil fuels. *Energies*, 15(2), 662.
- [6] Aamri, F. E., Maker, H., Sera, D., Spataru, S., Guerrero, J. M., Fakkar, A., & Mouhsen, A. (2023). Stability analysis for DC-link voltage controller design in single-stage single-phase grid-connected PV inverters. *IEEE Journal of Photovoltaics*.

- [7] Li, H., & Wei, H. (2023, December). High Voltage Ride-Through Control Strategy for Two-Stage PV Grid-Connected Systems. In 2023 2nd Asia Power and Electrical Technology Conference (APET) (pp. 688-692). IEEE.
- [8] Tak, N., Chattopadhyay, S. K., & Chakraborty, C. (2022). Single-sourced double-stage multilevel inverter for grid-connected solar PV systems. *IEEE Open Journal of the Industrial Electronics Society*, 3, 561-581.
- [9] Wang, Y., & Yu, X. (2013, November). Comparison study of MPPT control strategies for double-stage PV grid-connected inverter. In IECON 2013-39th Annual Conference of the IEEE Industrial Electronics Society (pp. 1561-1565). IEEE.
- [10] Yang, Y., Zhou, K., & Blaabjerg, F. (2015). Current harmonics from single-phase grid-connected inverters—Examination and suppression. *IEEE Journal of Emerging and Selected Topics in Power Electronics*, 4(1), 221-233.
- [11] Ding, G., Gao, F., Tian, H., Ma, C., Chen, M., He, G., & Liu, Y. (2015). Adaptive DC-link voltage control of two-stage photovoltaic inverter during low voltage ride-through operation. *IEEE Transactions on Power Electronics*, 31(6), 4182-4194.
- [12] Jain, C., & Singh, B. (2016). An adjustable DC link voltage-based control of multifunctional grid interfaced solar PV system. *IEEE Journal of Emerging and Selected Topics in Power Electronics*, 5(2), 651-660.
- [13] Zhou, X., Liu, Q., Ma, Y., & Xie, B. (2021). DC-link voltage research of photovoltaic grid-connected inverter using improved active disturbance rejection control. *IEEE Access*, 9, 9884-9894.
- [14] Townsend, C. D., Yu, Y., Konstantinou, G., & Agelidis, V. G. (2015). Cascaded H-bridge multilevel PV topology for alleviation of per-phase power imbalances and reduction of second harmonic voltage ripple. *IEEE Transactions on Power Electronics*, 31(8), 5574-5586.
- [15] Kan, S., Ruan, X., & Huang, X. (2022). Compensation of second harmonic current based on bus voltage ripple limitation in single-phase photovoltaic grid-connected inverter. *IEEE Transactions on Industrial Electronics*, 70(7), 7525-7532.
- [16] Dang, X., Pan, S., Pan, X., Gao, W., Ding, K., & Li, W. (2020, October). A modular three-phase photovoltaic inverter with elimination of phase unbalance and reduction of second harmonic voltage ripple. In IECON 2020 The 46th Annual Conference of the IEEE Industrial Electronics Society (pp. 1186-1191). IEEE.
- [17] Ismail, H. A., & Diab, A. A. Z. (2024). An efficient, fast, and robust algorithm for single diode model parameters estimation of photovoltaic solar cells. *IET Renewable Power Generation*.
- [18] Kim, Y. J., & Kim, H. (2019). Optimal design of LCL filter in grid-connected inverters. *IET Power Electronics*, 12(7), 1774-1782.
- [19] Ma, G., Xie, C., Li, C., Zou, J., & Guerrero, J. M. (2023). Passivity-Based Design of Passive Damping for LCL-Type Grid-Connected Inverters to Achieve Full-Frequency Passive Output Admittance. *IEEE Transactions on Power Electronics*.
- [20] Merai, M., Naouar, M. W., Slama-Belkhouja, I., & Monmasson, E. (2021). A systematic design methodology for DC-link voltage control of single phase grid-tied PV systems. *Mathematics and Computers in Simulation*, 183, 158-170.

- [21] Avci, E., & Ucar, M. (2020). Proportional multi-resonant-based controller design method enhanced with a lead compensator for stand-alone mode three-level three-phase four-leg advanced T-NPC inverter system. *IET Power Electronics*, 13(4), 863-872.
- [22] Alemi, P., Bae, C. J., & Lee, D. C. (2015). Resonance suppression based on PR control for single-phase grid-connected inverters with LLCL filters. *IEEE journal of emerging and selected topics in power electronics*, 4(2), 459-467.
- [23] Xie, Z., Chen, Y., Wu, W., Wang, Y., Gong, W., & Guerrero, J. M. (2021). Frequency coupling admittance modeling of quasi-PR controlled inverter and its stability comparative analysis under the weak grid. *IEEE Access*, 9, 94912-94922.